Master's Project – Final Report

THE APPLICATION OF HIGH-FREQUENCY MICROWAVES IN TISSUE ABLATION FOR CANCER TREATMENT

Student : Hung Thanh Luyen

Advisors : Professor Nader Behdad
Professor Susan C. Hagness

Department of Electrical and Computer Engineering

University of Wisconsin-Madison

Madison, Wisconsin, U.S.A., 2014

Abstract

The study demonstrates the feasibility of using high-frequency microwaves for tissue ablation by comparing the performance of a 10 GHz microwave ablation system with that of a 1.9 GHz system. Two sets of floating sleeve dipole antennas operating at these frequencies were designed and fabricated for use in *ex vivo* experiments with bovine livers. Combined electromagnetic and transient thermal simulations were conducted to analyze the performance of these antennas. Subsequently, a total of 16 ablation experiments (eight at 1.9 GHz and eight at 10.0 GHz) were conducted at a power level of 42 W for either 5 or 10 minutes. In all cases, the 1.9 GHz and 10 GHz experiments resulted in comparable ablation zone dimensions. Temperature monitoring probes revealed faster heating rates in the immediate vicinity of the 10.0 GHz antenna compared to the 1.9 GHz antenna, along with a slightly delayed onset of heating farther from the 10 GHz antenna, suggesting that heat conduction plays a greater role at higher microwave frequencies in achieving a comparably sized ablation zone. The results obtained from these experiments agree very well with the combined electromagnetic/thermal simulation results. These simulations and experiments show that using lower frequency microwaves does not offer any significant advantages, in terms of the achievable ablation zones, over using higher frequency microwaves. Indeed, it is demonstrated that high-frequency microwave antennas may be used to create reasonably large ablation zones. Higher frequencies offer the advantage of smaller antenna size, which is expected to lead to less invasive interstitial devices and may possibly lead to the development of more compact multi-element arrays with heating properties not available from single-element antennas.

1 Introduction

Microwave ablation (MWA) is being investigated for a variety of possible therapeutic applications (e.g. [1]-[7]). In MWA, an interstitial antenna is typically used to deliver microwave energy into the tissue and heat it up to temperature levels that result in immediate cell death. A number of studies have examined tissue ablation at microwave frequencies using different types of interstitial antennas (e.g. [7]-[20]). In most of these studies, the antenna is fed with a coaxial cable and the topology of the antenna and its feed structure are optimized to achieve the desired heating pattern while choking the currents flowing on the outer surface of the outer conductor of the feeding coaxial cable. Specific examples of these designs include the floating sleeve dipole [8], choke [9], triaxial [10], and cap-choke [14]-[15] antennas. While many different antenna types and designs have been examined for MWA, the vast majority of these studies share a common trait. Namely, they have examined MWA at frequencies below 2.5 GHz (e.g. [7]-[16]). In fact, most of the studies reported in this area to date have used frequencies around 915 MHz (e.g. [3]-[4], [15]-[16]) and 2.45 GHz (e.g. [5]-[14]) for ablation purposes.

A careful review of the literature in this area reveals only a few studies that have examined using higher frequencies for MWA applications. In [17], a 9.2 GHz endometrial ablation system was developed for treatment of abnormal menstrual bleeding; the frequency was chosen so that the total depth of heating matched the endometrial thickness [18]. In [19]-[20], a multi-functional antenna operating at 14.5 GHz was proposed for both tissue ablation and characterization and examined for treatment of liver cancer. The frequency 14.5 GHz was reported to be optimal for both high power ablation and low power characterization [19]. In [21], 18 GHz was identified as the optimum frequency in the 0.9-30 GHz range for MWA of xenografted mice tumors with high tissue specificity (low collateral damage) and high efficiency (low input power). These studies, however, are exceptions rather than the norm.

The widespread availability of high-power generators at 915 MHz and 2.45 GHz and the FCC allocation of those bands for industrial, scientific, and medical (ISM) use are two practical factors that have motivated the use of low frequencies in MWA. However, these are not limiting factors, as higher-frequency sources as well as higher-frequency ISM bands are readily available. In terms of technical considerations, the choice of low frequencies has been driven by concerns that smaller penetration depths at higher electromagnetic frequencies would preclude the creation of sufficiently large ablation volumes. In fact, factors other than frequency may have a greater influence on the effective penetration depth of microwave radiation from interstitial applicators [26]. However, assumptions about penetration-depth constraints have not been extensively tested.

In this study, we examine the use of higher frequency microwaves for tissue ablation and compare with lower frequency MWA performance. Two interstitial floating sleeve dipole (FSD) antennas operating at 10.0 GHz and 1.9 GHz are used in *ex vivo* ablation experiments conducted in fresh bovine livers. The antennas are based on the design reported in [8]. FSDs are easy to implement, provide localized specific absorption rate (SAR) patterns, and efficiently choke the currents flowing on the outer surface of the outer conductors of the feeding coaxial cables to avoid heating the tissue along the insertion path of the antennas. In both the 10 GHz and 1.9 GHz experiments, the same ablation time (5 or 10 min.) and input power level (42 W) are used. The dimensions of the ablation zones achieved at 10.0 GHz are found to be comparable to those achieved at 1.9 GHz. Additionally, the heating rates in the vicinity of the antenna are higher in the 10 GHz experiments than in the 1.9 GHz experiments.

These experimental results suggest that the penetration depth of propagating electromagnetic

waves in lossy biological tissues is not the most appropriate metric for determining the suitability (or lack thereof) of a given frequency for tissue ablation. Moreover, these results suggest that using a relatively low microwave frequency (such as 1.9 GHz) does not offer any advantages over using higher frequencies (on the order of 10.0 GHz) in terms of the ablation sizes that may be achieved. Using high-frequency microwaves, however, offers a number of practical advantages. Specifically, at higher frequencies, smaller and potentially less intrusive antennas may be used for tissue ablation. Furthermore, smaller antennas permit the design of compact multi-element arrays that may potentially generate heating patterns which are not easily achieved with a single low-frequency interstitial antenna.

2 Antenna Design and Simulation

Fig. 1 shows the longitudinal side view and the cross sectional view of the FSD antennas used in these experiments. Each antenna is composed of a main feeding coaxial cable with a dipole at the end. The dipole has arm lengths of h_a and h_b and a gap length of g. A floating sleeve with a length of h_s is used to choke the RF currents excited on the outer surface of the outer conductor of the feeding coaxial cable. This helps prevent the heating of tissue along the insertion path of the antennas and also makes the response of the antenna independent of the insertion depth into the tissue [8]. The entire structure is embedded in a Teflon catheter as shown in Fig. 1(a) and 1(b). Two sets of FSD antennas operating at 1.9 GHz and 10.0 GHz are designed for ablation experiments in bovine liver.

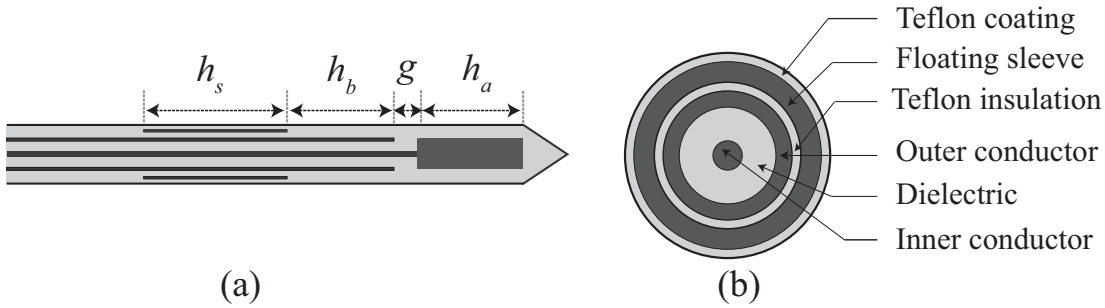

Figure 1: Topology of the floating sleeve dipole (FSD) antenna used in the ablation experiments. (a) Side view. (b) Cross-sectional view. The outer diameters of the various layers are as follows: inner conductor = 0.515 mm, dielectric = 1.676 mm, outer conductor = 2.2 mm, Teflon insulator = 2.5 mm, floating sleeve = 3.2 mm, Teflon coating = 3.5 mm.

For simulation purposes, the permittivity of bovine liver is modeled with the following one-pole Cole-Cole dispersion model:

$$\hat{\epsilon}(\omega) = \epsilon_\infty + \frac{\Delta\epsilon}{1 + (j\omega\tau)^{1-\alpha}} + \frac{\sigma_i}{j\omega\epsilon_0} \tag{1}$$

The Cole-Cole parameters (ϵ_∞, $\Delta\epsilon$, τ and σ_i) are determined from the following second-order polynomials that characterize the temperature dependence over the range from room temperature

to 60°C [22]:

$$\epsilon_\infty(T) = A_1T^2 + B_1T + C_1 \tag{2}$$
$$\Delta\epsilon(T) = A_2T^2 + B_2T + C_2 \tag{3}$$
$$\tau(T) = A_3T^2 + B_3T + C_3 \tag{4}$$
$$\sigma_i(T) = A_4T^2 + B_4T + C_4 \tag{5}$$

The values of the quadratic coefficients are given in Table I.

TABLE 1: QUADRATIC COEFFICIENTS FOR THE TEMPERATURE-DEPENDENT COLE-COLE PARAMETERS IN EQUATIONS (2)-(5)

	n	A_n	B_n	C_n
ϵ_∞	1	-0.0127	0.8610	-5.4119
$\Delta\epsilon$	2	0.0115	-0.8933	58.3598
τ [ps]	3	-0.0014	-0.0640	13.3749
σ_i [mS/m]	4	0.185	0.349	569.673

The specific absorption rate (SAR), defined as the power dissipated per unit volume $[\mathrm{W/m^3}]$ normalized by the tissue mass density $[\mathrm{kg/m^3}]$, provides a measure of the amount of microwave energy absorbed in the tissue. The spatial variation in SAR in the region of tissue surrounding the antenna is calculated for each of the two FSD antennas using full-wave computational electromagnetic simulations in CST Microwave Studio. The dimensions (h_a, h_b, h_s, and g) of each antenna are tuned to ensure that it is impedance matched and provides a localized SAR pattern at the desired frequency of operation. The final optimized dimensions of both antennas are provided in the caption of Fig. 1 and Table II. For additional details about the principles of operation of a FSD antenna, the reader is referred to [8].

TABLE 2: DIMENSIONS OF ANTENNA SEGMENTS SHOWN IN FIG. 1 FOR THE TWO FSD ANTENNA PROTOTYPES EXAMINED IN THIS STUDY.

	h_s[mm]	h_b [mm]	h_a [mm]	g [mm]
1.9 GHz	23.5	10.4	10.4	2
10 GHz	5.3	4	4	1

Fig. 2(a) and 2(b) show the normalized SAR in the vicinity of the 10.0 GHz and the 1.9 GHz FSD antennas, respectively. In both antennas, the SAR levels are reduced by at least 20 dB at the edge of the floating sleeve compared to the peak SAR value. This indicates that the floating sleeves effectively suppress the currents excited on the outer surface of the outer conductor of the feeding coaxial cable as indicated in [8]. Fig. 2(c) shows the -25 dB contours of both the 1.9 GHz and 10 GHz antennas plotted in the same graph, along with the outline of the catheter, to allow for direct comparison. We observe that the -25 dB contour for the SAR pattern of the 1.9 GHz antenna encompasses a larger volume compared to that of the 10.0 GHz antenna. This is indeed due to the larger penetration depth of electromagnetic waves at 1.9 GHz compared to

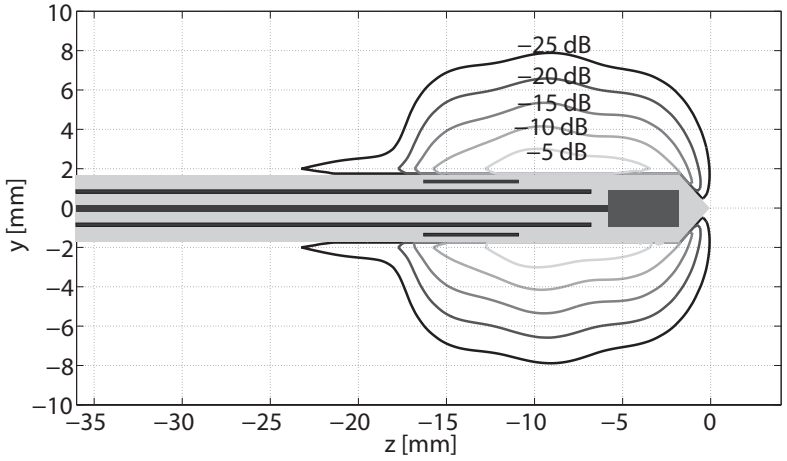

(a)

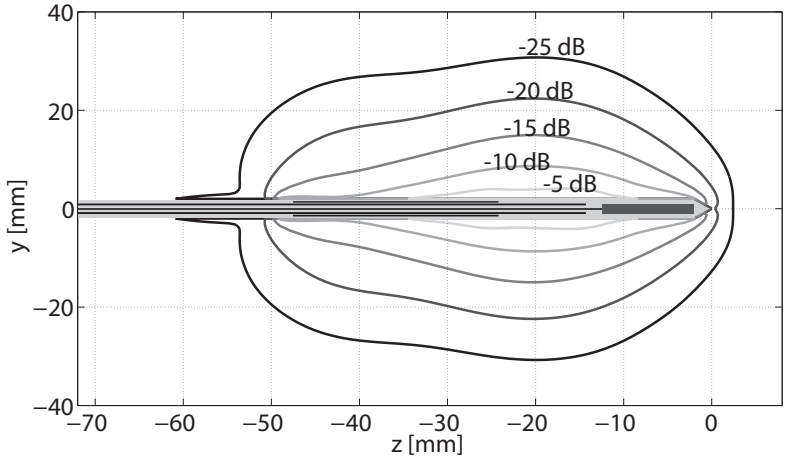

(b)

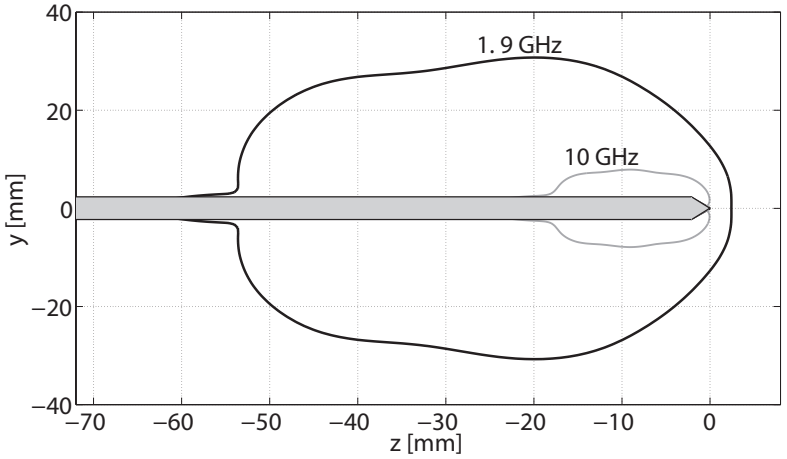

(c)

Figure 2: Simulated SAR patterns for the (a) 10.0 GHz and (b) 1.9 GHz FSD antennas examined in this study. (c) Direct comparison of the -25 dB contours of the 10 GHz (grey curve) and 1.9 GHz antennas (black curve).

that at 10.0 GHz. However, as will be shown later, this does not adversely affect the size of the ablation zones that may be achieved using the 10 GHz FSD antenna.

We also examined the expected heating patterns using combined electromagnetic/thermal simulations in CST Multiphysics Studio. The assumed thermal properties of copper, Teflon, liver, and air are listed in Table III. The thermal properties and mass density of liver are taken from [23]. First, we simulated the *ex vivo* case where there is no metabolic heat generation or blood perfusion. In these *ex vivo* simulations, the liver is assumed to be at room temperature (20°C) before ablation. Subsequently, in a second round of thermal simulations, we included the effects of metabolic heat generation and blood perfusion to simulate the *in vivo* performance of MWA at the two frequencies. We assumed a heat generation rate of 10.41 $\mathrm{W/kg}$ and blood perfusion rate of 1000 $\mathrm{ml/kg/min}$. For each simulation, the calculated microwave power dissipation per unit volume within the bovine liver, scaled for an input power of 42 W, is used as the external heat source.

In all of these simulations, the liver is modeled as a homogeneous tissue. Moreover, changes in the physical properties of tissue that occur during ablation (e.g. temperature-dependent dielectric properties) and thermodynamic mechanisms such as the latent heat of water vaporization are not taken into account. These will inevitably introduce some discrepancies between the results obtained in these simulations and those obtained from the *ex vivo* ablation experiments. Nonetheless, these simplified simulations do provide useful information about the relative performance of the 1.9 GHz and 10 GHz systems in both *ex vivo* and *in vivo* ablation scenarios.

TABLE 3: THERMAL PROPERTIES OF MATERIALS USED IN THERMAL SIMULATIONS

	Thermal conductivity [W/m.K]	Specific heat capacity [kJ/kg.K]	Heat diffusivity [$\mathrm{m^2/s}$] $\times 10^{-7}$
Liver	0.488	3.37	1.38
Copper	401	0.39	1151
Teflon	0.2	1	0.91
Air	0.026	1.005	214.8

Fig. 3 shows the results of the transient thermal simulation for the 10.0 GHz FSD antenna at different observation times after the start of the ablation procedure. Specifically, the graph shows the boundary of the 60°C temperature contours of the *ex vivo* (black curves) and the *in vivo* (red curves) simulation at different observation times. We chose 60°C, the median temperature of the congestive zone [24], to define the ablation zone boundary for the purpose of estimating the dimensions of the ablation zone. The temperature inside the volume bounded by each contour is higher than 60°C. Fig. 4 shows the results of a similar transient thermal simulation conducted for the 1.9 GHz FSD antenna. For each antenna, the high temperature regions first appear around the slot and arms and then expand as time increases. Upon comparing the results shown in Fig. 3(b) and Fig. 4(b) for both *ex vivo* and *in vivo* cases, we see that for shorter ablation times (e.g. 1 min.), the ablation zone provided by the 10 GHz antenna is larger than the one provided by the 1.9 GHz antenna. This larger ablation zone may be explained by examining the SAR patterns shown in Fig. 2. As shown in Fig. 2(c), the energy provided to the 10.0 GHz antenna is deposited in a smaller volume compared to the volume at 1.9 GHz. Therefore, the thermal energy density in the

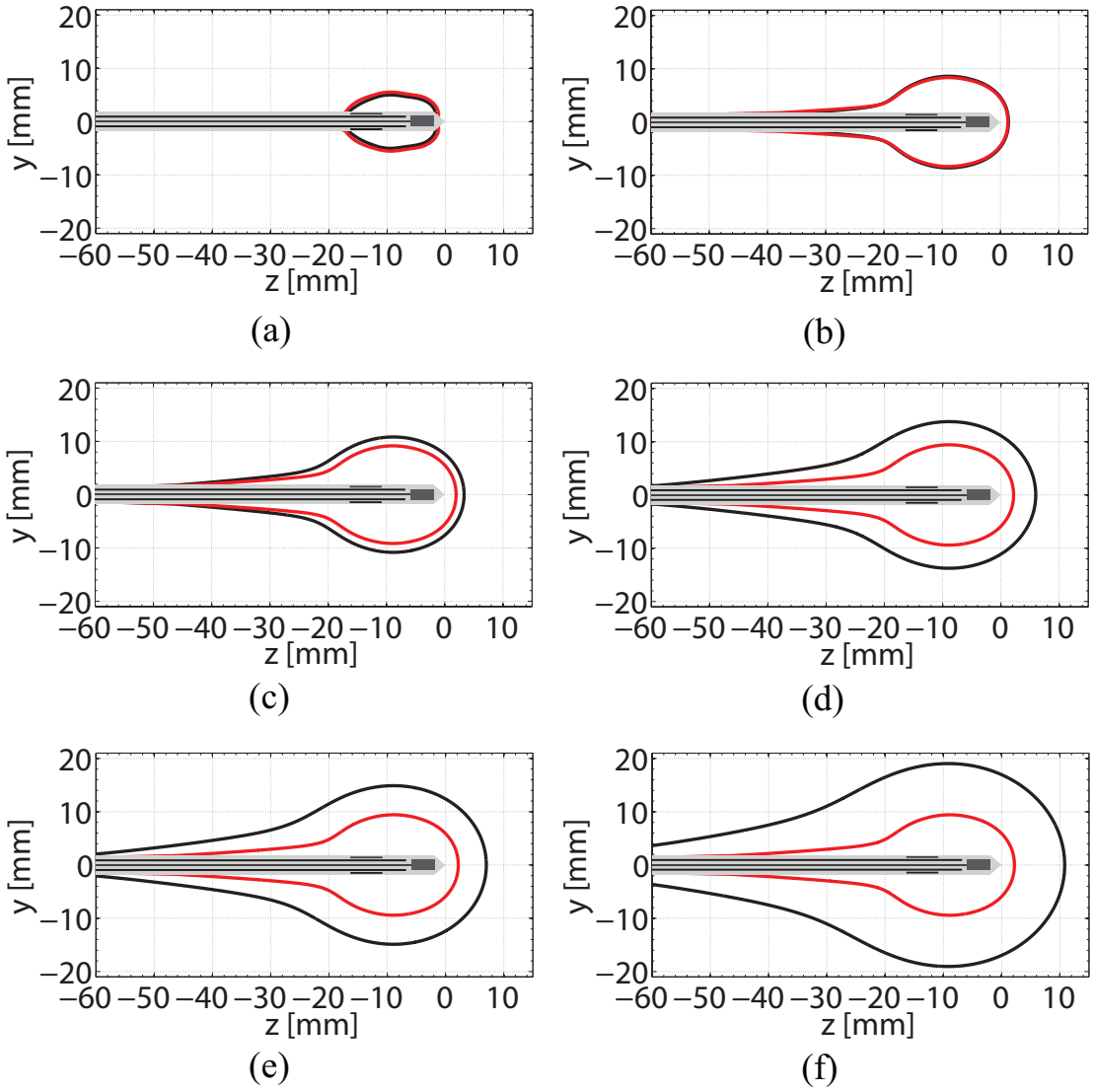

Figure 3: Transient thermal simulations show the expanding heating zone of the 10 GHz antenna at (a) 10 seconds, (b) 1 min., (c) 2 min., (d) 4 min., (e) 5 min., and (f) 10 min. The black contour represents the $60°C$ *boundary from the ex vivo simulation (no metabolic heat generation or blood perfusion). The red contour represents the* $60°C$ *boundary from the in vivo simulation (including the effects of metabolic heat generation and blood perfusion).*

vicinity of the 10 GHz antenna is higher, which results in a faster temperature rise compared to the 1.9 GHz case. As the ablation time increases, however, the sizes of the ablation zones in the *ex vivo* simulations of the two FSD antennas become comparable. This is particularly evident from the 5-min.-ablation results shown in Figs. 3(e) and 4(e) and the 10-min.-ablation results shown in Figs. 3(f) and 4(f). Thus, the large ablation volume of the 1.9 GHz antenna may be primarily attributed to the large volume in which this antenna deposits the input microwave energy (see Fig. 2(b)). For the 10 GHz antenna, however, the smaller energy deposition volume does not appear to adversely impact the size of the ablation zone, as experimentally confirmed in Section III. This is due to the thermal diffusion process that transfers heat from the direct-microwave-absorption areas in the immediate vicinity of the 10.0 GHz FSD antenna to the surrounding

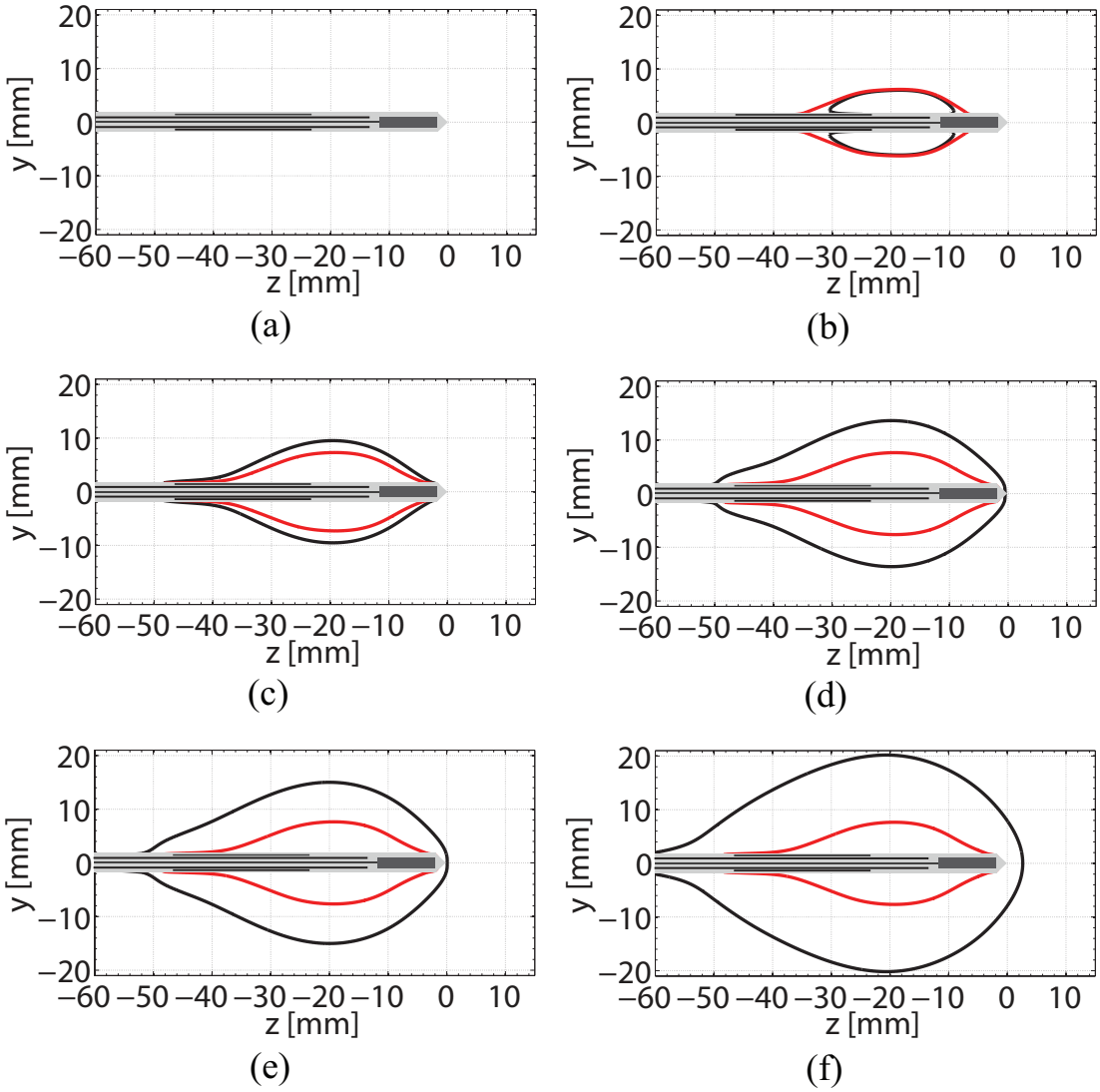

Figure 4: Transient thermal simulations show the expanding heating zone of the 1.9 GHz antenna at (a) 10 seconds, (b) 1 min., (c) 2 min., (d) 4 min., (e) 5 min., (f) 10 min. The black contour represents the $60°C$ *boundary from the ex vivo simulation. The red contour represents the* $60°C$ *boundary from the in vivo simulation.*

areas. Therefore, even though these distant regions do not absorb a significant part of the input microwave energy (see Fig. 2(a)), they nonetheless get hot enough to cause ablation on time scales that are comparable to (or even faster than) those associated with low-frequency MWA.

Comparison between the *ex vivo* and *in vivo* simulations of each antenna in Figs. 3 and 4 shows that the effect of blood perfusion has significant impact on the size of the achievable ablation zones at both frequencies. For both antennas, the *in vivo* ablation zones reach their steady-state dimensions after a short ablation time (e.g. 2 min.) and their largest short-axis diameters (measured on the y axis) achieved at the end of 10 min. are approximately half the size of those achieved in the *ex vivo* case. The cooling effects of the blood perfusion result in the reduction of the ablation zone dimensions for both the 1.9 GHz and the 10 GHz systems. However, the 10 GHz antenna, which delivers higher-density energy in the central heating zone,

creates a slightly larger ablation zone compared to the 1.9 GHz antenna as shown in Figs. 3 and 4.

3 Ablation Experiments

The 1.9 GHz and 10.0 GHz FSD antennas were fabricated out of 50 Ω UT-085C-LL semi-rigid coaxial cables from Micro-Coax. The floating sleeves were created from hollow copper tubes (the physical dimensions are provided in Fig. 1 and Table II). SMA connectors were attached to the feeding ends of the semi-rigid coaxial cables. The entire assembly was wrapped in Teflon tape according to the topology shown in Fig. 1. The overall length of the assembly, from the tip of the antenna to the end of the SMA connector, is 38 cm for each antenna.

Prior to beginning the ablation experiments, we measured the dielectric properties of the livers at room temperature over the frequency range of 500 MHz to 20 GHz using an Agilent vector network analyzer (E8364A) and an Agilent dielectric probe kit (85070E). In all cases, the dielectric properties were found to be similar to those used in our simulations, with the maximum difference less than 15%. We also measured the input VSWR of each antenna at different insertion depths into the liver using a vector network analyzer (Agilent E5071C). In all cases, the responses of the antennas at their desired frequency of operation did not change when the insertion depth was changed. This indicates that the floating sleeve baluns used in these antennas effectively suppress the currents excited on the outer surfaces of the outer conductors of the feeding coaxial cables. Moreover, we found the input VSWR to be consistently lower than 1.6, indicating a good impedance match in all cases. Immediately after each ablation experiment, we also measured the VSWR to determine whether the impedance match degraded due to ablation-induced changes in tissue dielectric properties. Fig. 5 shows the comparison between pre- and post-ablation VSWRs. While we do observe slight degradation, the post-ablation VSWRs were consistently below 1.8 in all cases. This demonstrates that a good impedance match was maintained for every antenna throughout the ablation process, despite significant changes in the dielectric properties of the tissue.

A total of 16 high-power ablation experiments were conducted in *ex vivo* bovine livers – four for each unique pairing of frequency (1.9 or 10.0 GHz) and ablation duration (5 or 10 min.). In all cases, the antennas were inserted at a depth of 13 cm into the bovine liver. For the 1.9 GHz experiments, a signal generator (HP 8350B Sweep Oscillator) connected to a high-power solid state amplifier (DMS 7066) was used as the source. The output of the power amplifier was connected to the input of the FSD antenna using a flexible coaxial cable. The input power level of the power amplifier was adjusted to achieve an output power level of 42 W (at the input of the semi-rigid coaxial cable). For the 10.0 GHz experiments, the same signal generator connected to a high-power traveling wave tube (TWT) amplifier (IFI T186-40) was used as the source. The output of the TWT amplifier was connected to the input of the antenna using a flexible coaxial cable. Similar to the previous case, the input power level of the TWT was adjusted to achieve an output power level of 42 W (at the input of the semi-rigid coaxial cable). During each ablation, the reflected power from the antenna was monitored and no significant changes in reflected power was detected, which agrees with the post-ablation VSWR measurements of each antenna.

During the ablation process, four fiber-optic temperature probes connected to a fluoroptic thermometer (Luxtron 3100) were placed in the vicinity of the antennas to monitor the temperature changes in the liver. The locations of the probes and their relative positions with respect

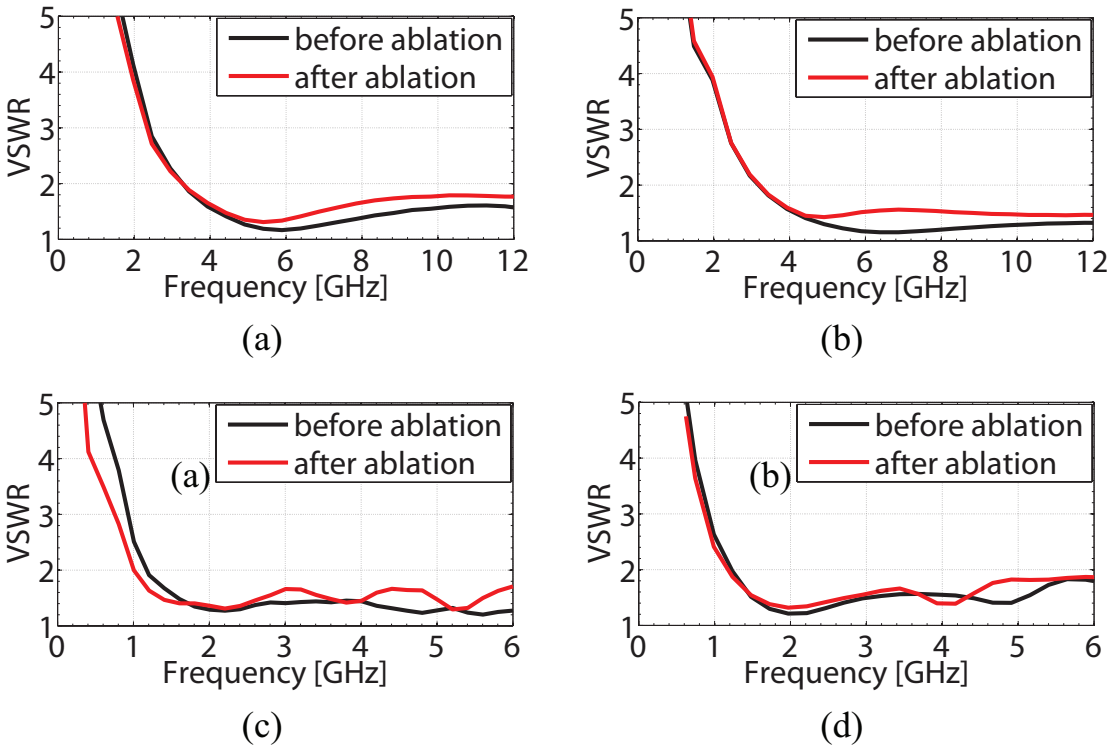

Figure 5: VSWR measurement results of (a) 10 GHz FSD antenna in 5-min.-ablation experiment, (b) 10 GHz FSD antenna in 10-min.-ablation experiment, (c) 1.9 GHz antenna in 5-min-ablation experiment, and (d) 1.9 GHz antenna in 10-min.-ablation experiment.

to the two antennas are shown in Figs. 6(a) and 6(b). Channels 1, 2, and 3 are placed along the radial direction at distances of 5, 10, and 15 mm from the antenna (similar to [25]). They are placed at the z coordinate (referring to Figs. 2, 3, and 4) that corresponds to the largest short-axis diameters (measured on the y axis) of both the SAR contours and the 60°C contours of each antenna. Channel 4 is placed at a distance of 10 mm beyond the tip of the dipole. A 3D-printed plastic guide was placed on top of the liver to hold the probes precisely at the desired positions. The plastic guide consists of an array of holes through which the temperature probes are routed, and parallel ridges to provide vertical support to the temperature probes as shown in Fig. 6(c). Each hole has a diameter of 1.8 mm to allow an 18-gauge needle to pass through. The needles were used to guide the temperature probes to the desired insertion depth from the top of the livers. Once each of the probes was guided to the desired location, the needle was removed from the hole leaving only the temperature probe inside the liver.

Fig. 7 shows representative temperature measurements for the 5- and 10-min.-ablation experiments at each frequency. Whenever a probe recorded a temperature level above 120°C (the maximum rated temperature for the probes), that probe was removed from the liver to protect it from being damaged. This was the case for Channel 1 temperature probes in all 10 GHz ablation experiments conducted (see Figs. 7(a) and 7(c)). A comparison of Channel 1 curves in Figs. 7(a) and 7(b) (or, similarly, in Figs. 7(c) and 7(d)) shows that the area immediately surrounding the antenna heats up much more rapidly for the 10 GHz system than the 1.9 GHz system. Furthermore, in most of the 10 GHz ablation experiments, the temperature readings of the more distant temperature probes (Channels 2, 3, and 4) remained flat for approximately the first 15-20

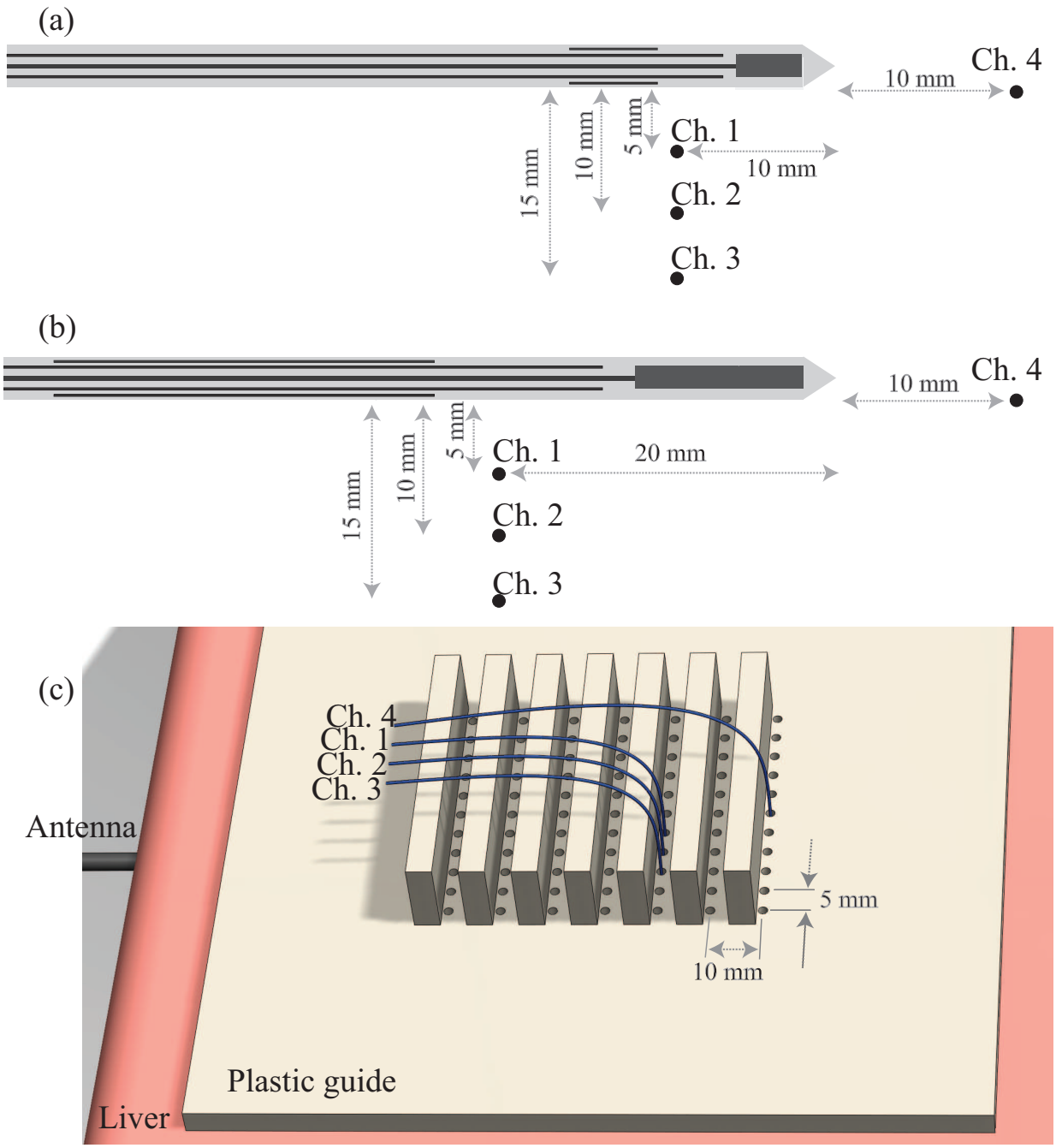

Figure 6: Positions of the four temperature probes. (a) Cross-sectional view (horizontal plane) of the 10.0 GHz antenna. (b) Cross-sectional view (horizontal plane) of the 1.9 GHz FSD antenna. (c) 3D view of the plastic guide used to position the probes.

seconds and then rapidly increased (e.g., compare Channels 2-4 of Fig. 7(a) and 7(b)). This is in contrast to the results we obtained for the 1.9 GHz system where in every experiment we conducted, all probes registered a rise in temperature as soon as the power was turned on. This observed delay in heating at locations away from the 10 GHz antenna suggests that ablation at 10 GHz is caused by intense localized heating in conjunction with indirect heating of the regions

away from the central heating zone. This is further supported by noting that the locations of the Channel 2, 3, and 4 probes fall outside of the -25 dB contour lines of the SAR pattern of the 10 GHz antenna (see Fig. 2(a)). This indicates that the amount of EM energy deposited in these areas is not significant and hence, heating at these locations is not direct. Possible mechanisms for this indirect heating include thermal diffusion and the movement of the generated water vapor from the intensely heated region to the surrounding areas. Since our simulations do not include the thermal effects of the generation and movement of steam and these simulations do predict similar behaviors as the ones shown in Fig. 7, we believe that the primary cause of this indirect heating is thermal diffusion effects.

It is also important to note a few exceptions to these general trends that were observed during our ablation experiments. For example, in Fig. 7(c) that shows the temperature levels for one of the 10-min ablation experiments conducted at 10 GHz, the temperature levels registered by Ch. 4 start to rise very rapidly and do not show the aforementioned 15-20 seconds delay which can be observed in Ch. 2-3 temperature levels. We explain this by pointing out that the liver is not a homogeneous environment (e.g., small veins are present at many locations within the liver). Specifically, in the case shown in Fig. 7(c), the locations of Ch. 1 and 4 sensors were near a small vein which connected them together. This vein acts as a conduit to transfer heat from the areas nearby the center of the antenna to locations close to Ch. 4 and explains why the temperature levels registered by Ch. 4 rise almost as fast as those registered by Ch. 1. Nonetheless, in the majority of the experiments, the temperature levels Ch. 2-4 showed the aforementioned delay that justifies our hypothesis that ablation in these locations is caused by heat diffusion. Irrespective of the heating mechanism (direct heating with EM waves or thermal diffusion), however, the temperature levels at all four locations reach the ablation threshold level (60°C) faster in the 10 GHz ablation system than that in the 1.9 GHz one. Finally, comparison of Figs. 7(a) and 7(c) with Figs. 7(b) and 7(d) shows that the 10 GHz ablation system provides significant heating in the areas beyond the tip of the antenna whereas the 1.9 GHz ablation system does not (e.g., see Ch. 4 curves in all of these figures).

Aside from these exceptions, the results and the trends observed in these measurements were found to be repeatable across experiments. This is demonstrated in Fig. 8. Figs. 8(a) and 8(b) show the average temperature values recorded at the four different observation locations for the 10 and 1.9 GHz ablation experiments, respectively. These results include data obtained from both the 5- and 10-minute ablation experiments. Therefore, the observation time for the average data is limited to 5 minutes. The bars show the standard deviations. The relatively large standard deviations are primarily attributed to the small total number of ablation experiments used to generate these results. Nonetheless, the same trends demonstrated in Fig. 7 and discussed earlier in this section are observable in these figures.

At the conclusion of each ablation experiment, the liver was cut along a plane through the insertion path of the antenna and the ablation zone was visually examined. The measured dimensions of each ablation zone, given by the maximum long- and short- axis diameters of the boundaries of the congestion zone, are reported in Table IV and Table V. The photographs of the ablation zones corresponding to the four experiments whose temperature measurements are shown in Fig. 7 are shown in Fig. 9. Figs. 9(a) and 9(b) show the ablation zones obtained after 5 minutes of ablation at respectively 10.0 GHz and 1.9 GHz. Figs. 9(c) and 9(d) show the ablation zones obtained after 10 minutes of ablation at respectively 10.0 GHz and 1.9 GHz. The results show that the dimensions of the ablation zones obtained at 10.0 GHz are comparable to those obtained at 1.9 GHz. Additionally, the photographs shown in Fig. 9 show that the ablation zones

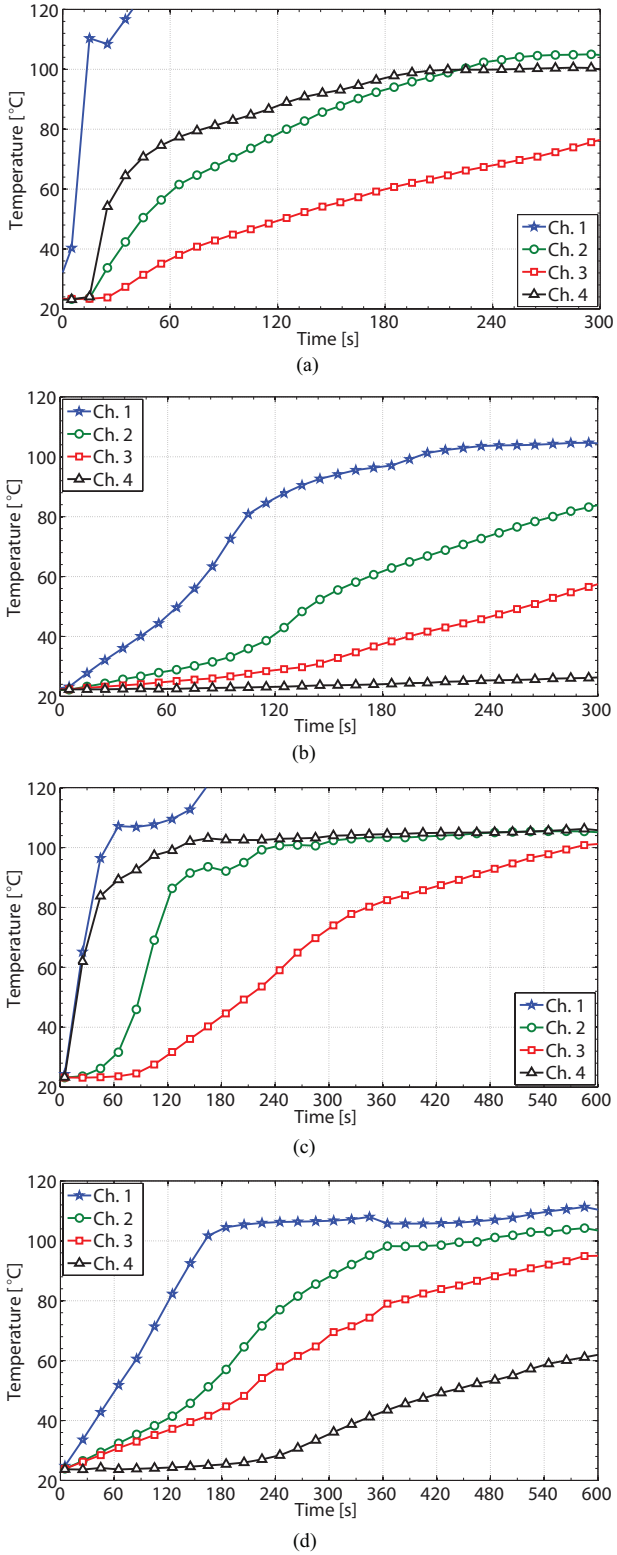

Figure 7: Temperature recorded by four temperature probes during the ablation experiments. (a) 10 GHz antenna, 5 min. ablation, (b) 1.9 GHz antenna, 5 min. ablation, (c) 10 GHz antenna, 10 min. ablation, and (d) 1.9 GHz antenna, 10 min. ablation.

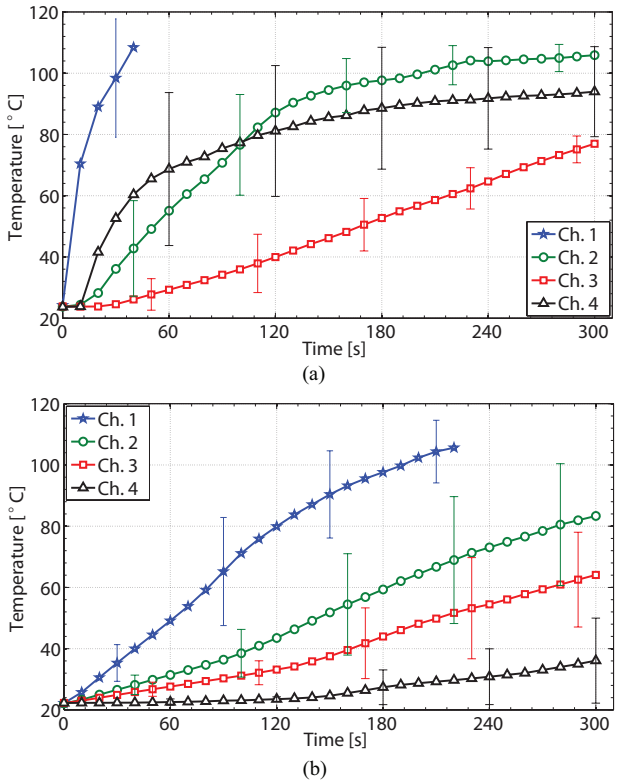

Figure 8: Average temperature values recorded at each channel during the first 5 minutes of all of the (a) 10 GHz and (b) 1.9 GHz ablation experiments. The bars show standard deviations. When a temperature level recorded by any of the sensors reached 120°, that sensor was removed from the ablation zone to avoid damaging it. Therefore, the data plotted for Ch. 1 is terminated before 5 minutes.

in the 10 GHz ablation experiments extend farther beyond the tips of the antennas, as confirmed by the temperature measurements of Ch. 4 in Fig. 7. Moreover, the size of the charred region in the vicinity of the 10 GHz antennas is slightly larger than that of the 1.9 GHz antenna. This agrees with the higher temperatures measured at Ch. 1 in the 10 GHz experiments in Fig. 7.

4 Conclusions

Our numerical and experimental studies presented in this report demonstrate the feasibility of using higher-frequency microwaves for tissue ablation. In particular, we demonstrated that, despite an increase in frequency by a factor of five, the sizes of the ablation zones obtained in 10 GHz MWA experiments are comparable to those achieved at 1.9 GHz conducted at the same power level and for the same duration. This is contrary to the widely accepted argument that lower-frequency microwaves provide larger ablation sizes due to higher penetration depths of electromagnetic waves into the body and the lower losses in biological tissues at such frequencies. Our experiments show that, as far as ablation size is concerned, MWA using a relatively low frequency of 1.9 GHz does not have any significant advantages over MWA using a relatively high frequency of 10.0 GHz. However, higher frequency microwaves offer the advantage of smaller antenna lengths. Additionally, new antenna topologies are currently under investigation that allow for eliminating coaxial baluns in high-frequency, coaxial-cable-fed MWA antennas

TABLE 4: ABLATION ZONE GENERATED WITH 1.9 GHZ AND 10 GHZ ANTENNAS FOR 5-MINUTE ABLATION TIMES

Frequency [GHz]	Size		Photograph
	Maximum long-axis diameter [cm]	Maximum short-axis diameter [cm]	
10	7.0	3.2	
10	5.5	3.3	
10	5.5	3.0	Fig. 8(a)
10	5.0	3.0	
1.9	5.7	3.5	
1.9	5.5	3.0	Fig. 8(b)
1.9	5.0	3.0	
1.9	5.1	2.8	

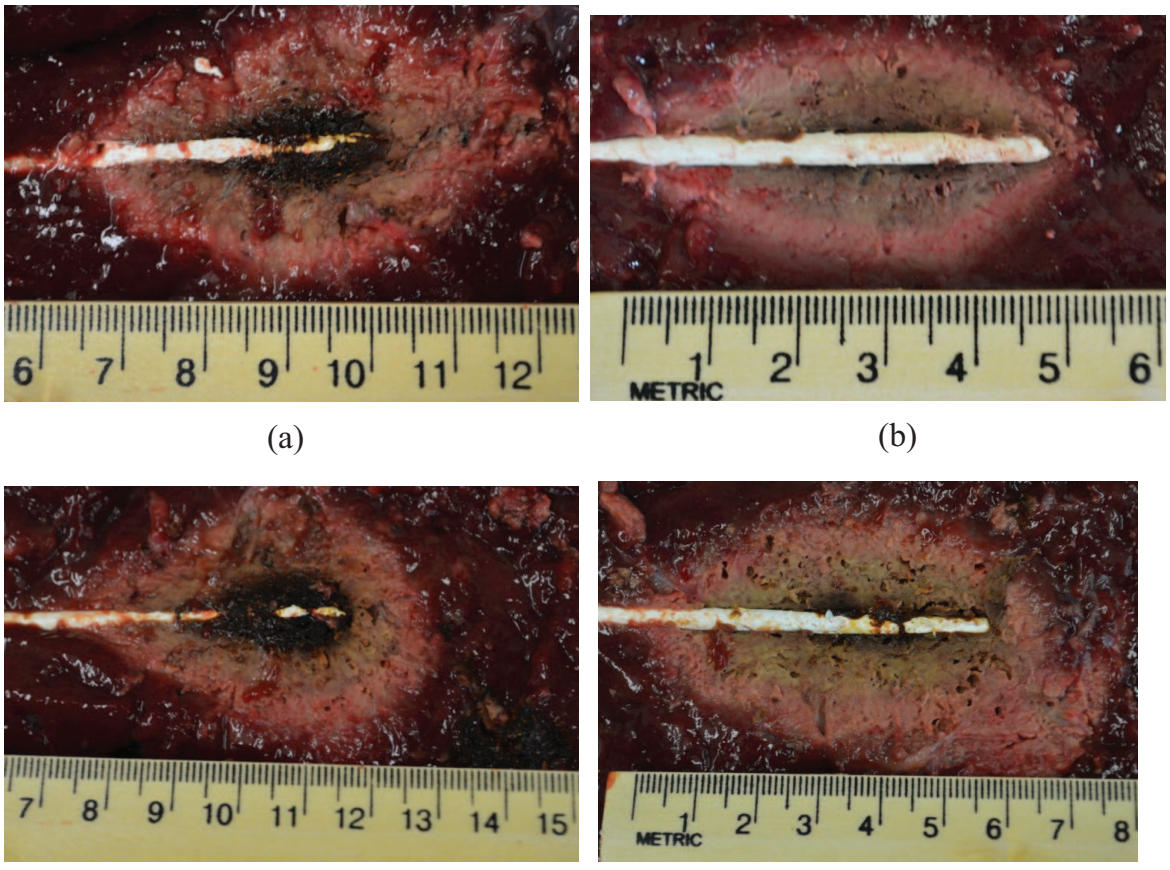

(a) (b)

(c) (d)

Figure 9: Photographs of the ablation zone obtained using 42 W of microwave power at (a) 10.0 GHz for 5 min., (b) 1.9 GHz for 5 min., (c) 10.0 GHz for 10 min., and (d) 1.9 GHz for 10 min.

TABLE 5: ABLATION ZONE GENERATED WITH 1.9 GHZ AND 10 GHZ ANTENNAS FOR 10-MINUTE ABLATION TIMES

Frequency [GHz]	Size		Photograph
	Maximum long-axis diameter [cm]	Maximum short-axis diameter [cm]	
10	6.4	4.0	
10	7.2	4.2	
10	7.0	3.8	
10	6.0	4.0	Fig. 8(c)
1.9	7.3	3.8	
1.9	6.5	3.5	Fig. 8(d)
1.9	7.0	3.7	
1.9	6.7	3.5	

thereby reducing the antenna diameter in addition to the antenna length. Therefore, MWA may potentially be performed using less invasive antennas at higher frequencies. Furthermore, using higher microwave frequencies, it may be possible to develop compact multi-element arrays that are capable of generating heating zones not achievable from large single-element antennas used in conventional low frequency MWA. Finally, in situations where a small ablation zone may be needed, using higher frequencies allows for the desired ablation size to be created in a shorter period of time. Due to these possible advantages, further investigation into using high-frequency microwaves for ablation experiments and studying new antenna designs and antenna arrays that take advantage of the unique properties offered at such high frequencies is indeed warranted.

Acknowledgment

We would like to thank Mr. Robert Weyker in the Meat Science Laboratory at the University of Wisconsin-Madison for providing us with bovine livers for the experiments reported in this project.

References

[1] C. J. Simon, D. E. Dupuy, and W. W. Mayo-Smith, "Microwave ablation: Principles and applications," *RadioGraphics*, vol. 25, pp. S69-S83, 2005.

[2] C. L. Brace, "Microwave tissue ablation: Biophysics, technology and applications," *Crit. Rev. Biomed. Eng.*, vol. 38, no. 1, pp. 65-78, 2010.

[3] G. Carrafiello, A. M. Ierardi, F. Piacentino, N. Lucchina, G. Dionigi, S. Cufarri, and C. Fugazzola, "Microwave ablation with percutaneous approach for the treatment of pancreatic adenocarcinoma," *Cardiovasc. Intervent. Radiol.*, vol. 35, no. 2, pp. 439-442, Apr. 2012.

[4] M. Cheng, M. A. Haider, M. J. Dill-Macky, J. M. Sweet, J. Trachtenberg, and M. R. Gertner, "MRI and contrast-enhanced ultrasound monitoring of prostate microwave focal thermal therapy: An in vivo canine study," *J. Magn. Reson. Im.*, vol. 28, no. 1, pp. 136-143, Jul. 2008.

[5] W. Zhou, X. Zha, X. Liu, Q. Ding, L. Chen, Y. Ni, Y. Zhang, Y. Xu, L. Chen, Y. Zhao, and S. Wang, "US-guided percutaneous microwave coagulation of small breast cancers: A clinical study," *Radiology*, vol. 263, no. 2, pp. 364-373, May 2012.

[6] Y. Kanaoka, C. Yoshida, T. Fukuda, K. Kajitani, and O. Ishiko, "Transcervical microwave myolysis for uterine myomas assisted by transvaginal ultrasonic guidance," *J. Obset. Gynaecol. Res.*, vol. 35, no. 1, pp. 145-151, Feb. 2009.

[7] M. Kuang, M. D. Lu, X. Y. Xie, H. X. Xu, L. Q. Mo, G. J. Liu, Z. F. Xu, Y. L. Zheng, and J. Y. Liang, "Liver cancer: Increased microwave delivery to ablation zone with cooled-shaft antenna—Experimental and clinical studies," *Radiology*, vol. 242, no. 3, pp. 914-924, 2007.

[8] D. Yang, J. M. Bertram, M. C. Converse, A. P. O'Rourke, J. G. Webster, S. C. Hagness, J. A. Will, and D. M. Mahvi, "A floating sleeve antenna yields localized hepatic microwave ablation," *IEEE Trans. Biomed. Eng.*, vol. 53, no. 3, pp. 533-537, Mar. 2006.

[9] I. Longo, G. B. Gentili, M. Cerretelli, and N. Tosoratti, "A coaxial antenna with miniaturized choke for minimally invasive interstitial heating," *IEEE Trans. Biomed. Eng.*, vol. 50, no. 1, pp. 82-88, Jan. 2003.

[10] C. L. Brace, P. F. Laeseke, and D. W. van der Weide, "Microwave ablation with a triaxial antenna: Results in ex vivo bovine liver," *IEEE Trans. Microw. Theory Tech.*, vol. 53, pp. 215-220, 2005.

[11] A. U. Hines-Peralta, N. Pirani, P. Clegg, N. Cronin, T. P. Ryan, Z. Liu, and S. N. Goldberg, "Microwave ablation: Results with a 2.45-GHz applicator in ex vivo bovine and in vivo porcine liver," *Radiology*, vol. 239, no. 1, pp. 94-102, 2006.

[12] K. Saito, S. Hosaka, S.-Y. Okabe, H. Yoshimura, and K. Ito, "A proposition on improvement of a heating pattern of an antenna for microwave coagulation therapy: Introduction of a coaxial-dipole antenna," *Elec. Commun. Jpn.*, vol. 86, no. 1, pp. 16-23, 2003.

[13] S. Labonte, A. Blais, S. R. Legault, H. O. Ali, and L. Roy, "Monopole antennas for microwave catheter ablation", *IEEE Trans. Microw. Theory Tech.*, vol. 44, No. 10, pp. 1832-1840, Oct. 1996.

[14] J. C. Lin and Y. Wang, "The cap-choke catheter antenna for microwave ablation treatment," *IEEE Trans. Biomed. Eng.*, vol. 43, pp. 657-660, Jun. 1996.

[15] S. Pisa, M. Cavagnaro, P. Bernardi, and J. C. Lin, "A 915-MHz antenna for microwave thermal ablation treatment: Physical design, computer modeling and experimental measurement," *IEEE Trans. Biomed. Eng.*, vol. 48, no. 5, pp. 599-601, May 2001.

[16] W. Hurter, F. Reinbold, and W. J. Lorenz, "A dipole antenna for interstitial microwave hyperthermia," *IEEE Trans. Microw. Theory Tech.*, vol. 39, no. 6, pp. 1048-1054, Jun. 1991.

[17] D. A. Hodgson, I. B. Feldberg, N. Sharp, N. Cronin, M. Evans, and L. Hirschowitz, "Microwave endometrial ablation: Development, clinical trials and outcomes at three years," *Br. J. Obstet Gynaec*, vol. 106, pp. 684-694, Jul. 1999.

[18] S. A. Jack, and K. G. Cooper, "Microwave endometrial ablation: an overview,", *Reviews in Gynaecological Practice*, vol. 5, pp. 32-38, 2005.

[19] R. P. Jones, N. R. Kitteringham, M. Terlizzo, C. Hancock. D. Dunne, S. W. Fenwick, G. J. Poston, P. Ghaneh, and H. Z. Malik, "Microwave ablation of ex vivo human liver and colorectal liver metastates with a novel 14.5 GHz generator," *Int. J. Hyperther.*, vol. 28, no. 1, pp. 43-54, 2012.

[20] C. P. Hancock, N. Dharmasiri, M. White, and A. M. Goodman, "The design and development of an integrated multi-functional microwave antenna structure for biological applications," *IEEE Trans. Microw. Theory Tech.*, vol. 61, no. 5, pp. 2230-2241, May 2013.

[21] J. Yoon, J. Cho, N. Kim, D. Kim, E. Lee, C. Cheion, and Y. Kwon, "High-frequency microwave ablation method for enhanced cancer treatment with minimized collateral damage," *Int. J. Cancer*, vol. 129, pp. 1970-1978, 2011.

[22] M. Lazebnik, M. C. Converse, J. H. Booske, and S. C. Hagness, "Ultrawideband temperature-dependent dielectric properties of animal liver tissue in the microwave frequency range," *Phys. Med. Biol.*, vol. 51, pp. 1941-1955, 2006.

[23] F. A. Duck, *Physical Properties of Tissue: A Comprehensive Reference Book*. London, Academic Press, 1990.

[24] J. Chiang, P. Weng, and C. L. Brace, "Computational modeling of microwave tumour ablation," *Int. J. Hyperther.*, vol. 29, no. 4, pp. 308-317, 2013.

[25] A. Andreano and C. L. Brace, "A comparison of direct heating during radiofrequency and microwave ablation in ex vivo liver," *Cardiovasc. Intervent. Radiol.*, vol. 36, pp. 505-511, 2013.

[26] J. Vrba, C. Fraconi, and M. Lapes, "Theoretical limits for the penetration depth of intracavitary applicators," *Int. J. Hyperther.*, vol. 12, no. 6, pp. 737-742, 1996.